Transverse tectonics feature delineated by modelling of magnetotelluric data from Garhwal Himalaya corridor, India

M. Israil[1,*], Paramjeet Mamoriya[1], Pravin K. Gupta[1] and S. K. Varshney[2]

[1]Indian Institute of Technology Roorkee, Roorkee 247 667, India
[2]Department of Science and Technology, New Mehrauli Road, New Delhi 110 016, India

We analyse magnetotelluric data recorded in the Garhwal Himalaya corridor, India, to study dimensionality and strike direction of the geoelectric structure. The geoelectric structure dimensionality in the corridor shows spatial variation with period. Geoelectric strike directions of the main Himalayan thrusts associated with the main arc – Main Frontal Thrust, Main Boundary Thrust and Main Central Thrust – are N72°W ± 8°, N70°W ± 3° and N71°W ± 6° respectively. Cross-strike directions oriented transverse and oblique with respect to the main arc geometry are also delineated. Transverse feature is constrained using 3D modelling.

Keywords: Three-dimensional modelling, dimensionality, magnetotelluric data, transverse tectonics.

THE Himalaya is one of the youngest and highest mountain ranges, which originated from continental collision tectonics and underthrusting of the Indian Plate beneath the Eurasian Plate. Regional N–S compression caused crustal shortening, horizontal extrusion and lithospheric delamination[1,2]. In this process, leading upper brittle portion of the subducting Indian crust has been sliced and stacked up southwards to form the Himalayan mountain belt. The Himalayan system is normally considered as laterally continuous along its arc[1]. However, Valdiya[3] pointed out large-scale fracture, fault and folds trending normal and oblique to the Himalayan tectonics trend. Undersurface extension of the Aravalli into the Lesser Himalaya was first postulated by Auden[4]. On the basis of along-strike variations in topography and relief, and the rate of convergence and shortening rates[5–9], the Himalayan arc was characterized into transverse zones that separate the mountain range into sectors with distinct thicknesses of major sedimentary units, deformation style and present-day seismicity. Mitra *et al.*[10] speculated that the Delhi–Haridwar basement ridge divides the lateral variations in the felsic component of the upper–middle Indian crust under the Ganga Basin. Khattri and Tyagi[11] using seismological data, explained the existence of oblique and transverse tectonics features in the Garhwal Himalayan region. Accordingly, the dominant structural trend is along the Himalayan mountain axis which swings from northwest in the western side to northeast trend in the east. A number of faults having strikes at high angles with the main Himalayan axis arc were identified. Some of these trend in NE–SW direction and have been postulated as continuation of the Aravalli trend into the Himalaya[11]. Recently, Godin and Harris[12] discussed using gravity data and their relationship to upper crustal faults, basement cross-strike discontinuities in the Indian crust beneath the Himalayan orogen. Existence of a transverse conductor has been explained on the basis of geomagnetic induction response[13] and is called the Trans-Himalayan Conductor (THC), which follows the strike of the Aravalli range of the Indian shield. Transverse tectonics in the Sikkim Himalaya was explained by Manglik *et al.*[14] on the basis of magnetotelluric (MT) studies. The geoelectric strike directions delineated in the MT data are consistent with the seismotectonic model of the Sikkim Himalaya. The model was obtained on the basis of focal mechanisms of moderate earthquakes and composite fault plane solutions of microearthquakes. In the present article, we analyse MT data to study, in terms of dimensionality and directionality, the oblique and transverse tectonics features and determine geoelectric strike directions in the Garhwal Himalayan Corridor (GHC). Further, a 3D geoelectrical model generated by integration of dimensionality and tipper responses has been presented.

Geology of the study area

The study area is located in Uttarakhand and MT data were recorded along the Roorkee–Gangotri (RKG) profile. Figure 1 shows the location of MT and tipper data sites. We shall refer to this section along the profile as Garhwal Himalayan corridor (GHC) in subsequent discussions; Geologically, the GHC is divided into four concentric litho-tectonic domains, separated by three south-verging thrusts. The Main Frontal Thrust (MFT), the southernmost tectonic boundary in the Himalaya, demarcates the

*For correspondence. (e-mail: mohammad.israil@gmail.com)

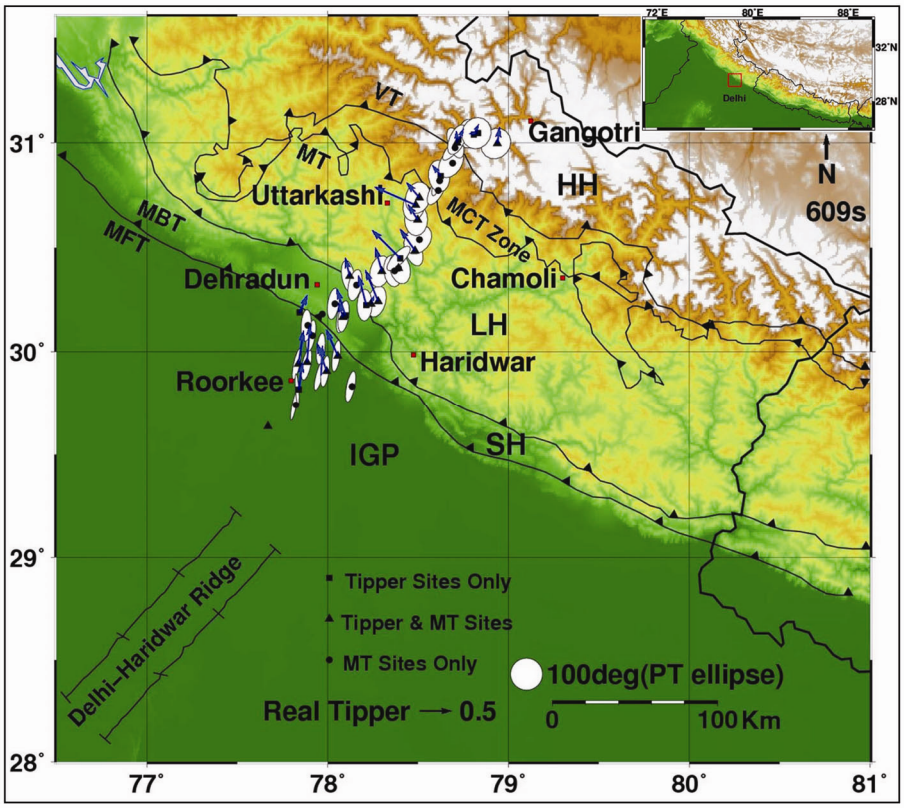

Figure 1. Location map of the study area showing magnetotelluric (MT) and tipper sites on a simplified tectonic map. Also plotted are the phase tensor ellipses and real induction arrows at representative period (609 s) in Weise convention at sites where tipper data are available. VT, Vaikrita thrust; MT, Munsiari thrust; MBT, Main Boundary Thrust; MFT, Main Frontal Thrust; IGP, Indo Gangetic Plain; SH, Sub Himalaya; LH, Lesser Himalaya; HH, Higher Himalaya (compiled from Valdiya[15] and Mahesh *et al.*[19]).

contact between the Indo-Gangetic alluvium to the south and the Sub-Himalaya to the north[15]. The Sub-Himalaya begins to the north of the MFT with an average elevation of 600 m, and rises abruptly above the Indo-Gangetic Plain (IGP) along the MFT. The Sub-Himalaya predominantly consists of 5–6 km thick tertiary and quaternary sediments. The Lesser Himalayan (LH) domain, which follows on the north, has an average elevation of 2500 m with profile elevation increasing towards the north. The LH domain largely consists of Precambrian rocks that are folded and fractured[1]. This domain is separated from the Sub-Himalaya (SH) by the north-dipping Main Boundary Thrust (MBT), which hades northwards[11,16] at 30–40°. The next major thrust is the Main Central Thrust (MCT) in the north. In the study area, the MCT zone is bounded by the Munsiari Thrust (MT) in the south and Vaikrita Thrust (VT) in the north[17–19]. The northernmost region of the profile is the Higher Himalayan (HH) crystalline zone containing most of the famous peaks of the mountain range and has an average elevation of 4500 m. In the study area, the dominant structural trend of the main Himalayan thrusts: MFT, MBT and MCT is northwest. A number of faults and other structural features that have strike in NE–SW direction have been postulated. An example of such a feature is the extension of northeast-trending Aravalli[11]. Auden[4] first indicated the rejuvenation of the Aravalli Mountain which, he believed, extended northeastward into the Himalaya. Prolongation of the Aravalli in the NNE–SSW direction towards Garhwal is also reflected in gravity anomaly[20]. Recently, the cross-strike discontinuities in the Indian crust beneath the Himalaya have been studied by Godin and Harris[12] using gravity data. They have explained the northern limit of cross-structure under the Himalaya.

Structure dimensionality and geoelectric strike

Determination of geoelectric structure dimensionality and directionality is an import step in MT data analysis and interpretation; it is the main focus of the present study. The data recorded from GHC were corrupted to different degrees by distortion due to different types of geological and man-made noise sources. To deal with noisy data, we used impedance invariants and phase tensor-based techniques for the determination of geoelectric dimensionality and strike directions[21,22]. The basic philosophy of the technique is discussed here briefly. The MT impedance

Table 1. Dimensionality criteria modified after Martí *et al.*[23]

Case	Criterion	Geoelectric dimensionality
1	$I_3 = I_4 = I_5 = I_6 = 0$	1D
2	$I_3 \neq 0$ or $I_4 \neq 0$; $I_5 = I_6 = 0$; $I_7 = 0$ or Q = 0	2D
3a	$I_3 \neq 0$ or $I_4 \neq 0$; $I_5 \neq 0$; $I_6 = 0$; $I_7 = 0$	3D/2D twist 2D affected by galvanic distortion (only twist)
3b	$I_3 \neq 0$ or $I_4 \neq 0$; $I_5 \neq 0$, $I_6 = 0$; Q = 0	3D/1D or 2D Galvanic distortion over a 1D or 2D structure (non-recoverable strike direction)
3c	$I_3 \neq 0$ or $I_4 \neq 0$; $I_5 = 0$,$I_6 = 0$; $I_7 = 0$ or Q = 0	3D/1D or 2D Galvanic distortion over a 1D or 2D structure resulting in a diagonal MT tensor
3d	$I_3 \neq 0$ or $I_4 \neq 0$; $I_5 \neq 0$; $I_6 \neq 0$ and $I_7 = 0$	3D/2D General case of galvanic distortion over a 2D structure
4	$I_7 \neq 0$	3D (affected or not affected by galvanic distortion)
5	Any or all of I_3, I_4, I_5 or I_6 is undefined.	Undetermined dimensionality, dimensionality not estimated (NE)

tensor can be written as a linear relationship between the orthogonal horizontal components of electric (E) and magnetic (H) fields as:

$$\begin{bmatrix} E_x \\ E_y \end{bmatrix} = \begin{bmatrix} Z_{xx} & Z_{xy} \\ Z_{yx} & Z_{yy} \end{bmatrix} \begin{bmatrix} H_x \\ H_y \end{bmatrix}, \quad (1)$$

where E_x, E_y, H_x, H_y and Z_{ij} are the components of electric and magnetic fields, and impedance tensor respectively. Weaver *et al.*[21] have developed dimensionality criteria based on seven rotational invariants (I_1 to I_7).

These criteria were modified by Martí *et al.*[23]. We modified these criteria further, in view of data quality (Table 1).

We have developed an algorithm in Matlab environment and implemented these criteria to determine the dimensionality in MT data recorded in the GHC. Figure 2 shows the dimensionality of geoelectric structure in the corridor along the profile. Data affected by galvanic distortion and 3D conductivity structure are grouped into four cases mentioned in Table 1 as '3a', '3b', '3c' and '3d'. This method cannot be applied to the impedance tensor having very large error (>30%) or $I_7 > 1$, and thus dimensionality cannot be estimated for such data points. In Figure 2, these regions are shown in red and are indicated as 'NE' on dimensionality scale.

In the period >2 s, major region along the profile is represented by 2D structure (Figure 2). The southern region, in the short period range (<2 s), is the IGP sedimentary section represented by layered (1D) structure. Phase tensor ellipse[22] in the short-period band reduced to a circle with less than 5° phase difference between minimum to maximum phase[22]. Underneath the IGP, only at longer periods (>2 s), and for majority of northern regions, for all periods, the structure is 2D while it is 3D only for a few localized regions. For the 2D region, we have estimated geoelectric strike direction. Three approaches – Groom–Bailey[24], Bahr[25,26] and phase tensor[22] – were used to determine consistent average strike directions in the four lithotectonic zones. These methods generate the geoelectric strike directions with 90° ambiguity. This ambiguity has been removed by constraining the strike direction to be consistent with the main Himalayan arc (northwest–southeast) in the region[27]. Phase tensor-based method is considered to be more accurate for determination of geoelectric strike direction due to the fact that phase is not affected by small-scale electric distortions[22]. We have recalculated strike for the entire data and observed that strike directions obtained using phase tensor method[22] are consistent. Figure 1 shows phase tensor ellipse along with induction arrows plotted in the Weise convention at representative period (609 s). It can be seen that the major axis of the ellipses are consistently oriented approximately in north–south direction at 15 sites located mainly in the southern zone of the profile. However, induction arrows at these sites are not aligned along the axis of the ellipse. On the contrary, induction arrows are generally oriented towards northwest, indicating conducting body in southeast and almost parallel to the MT profile. Anomalous behaviour of induction arrows has also been explained by Arora and Adam[13]: 'because of the superposition of the fields of two or more bodies with non-parallel strikes, the induction arrow pattern becomes complex and ambiguous'.

In 216 data points in the period band of 13–1024 s, phase tensor ellipses show N13°E average geoelectrical strike direction in southern region at 15 sites. Since this consistently appeared in a large number of sites and data points, it cannot be ignored for this dataset. It has been found that a consistent dominant geoelectrical strike direction in the southern region at periods greater than 13 s is N13°E. This was also observed in an earlier work[28], where it was modified using the 90° ambiguity in

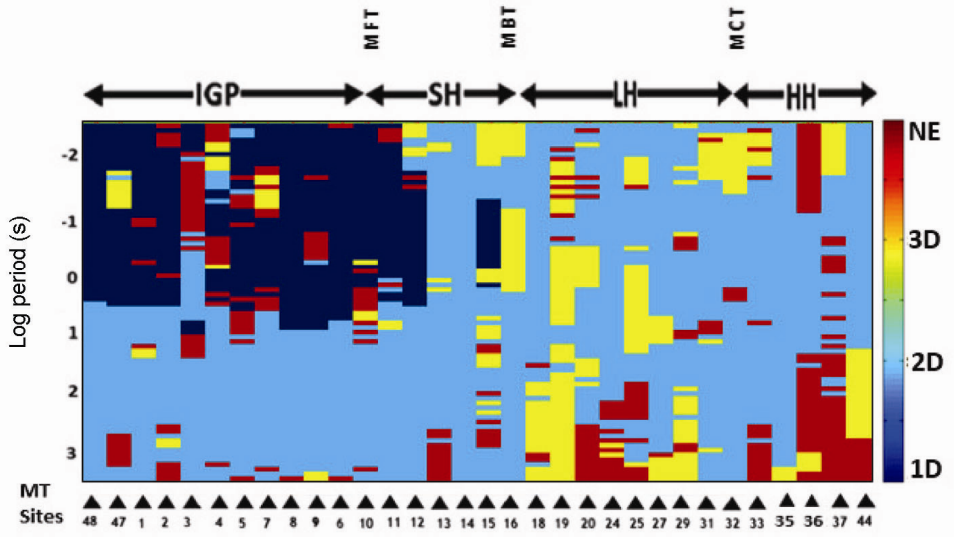

Figure 2. Geoelectric structure dimensionality variations with period in the Garhwal Himalayan corridor along the MT profile. NE on colour scale indicates that dimensionality criteria cannot be used for this region.

view of the main Himalayan arc configuration (northwest–southeast). However, the geological literature also suggests the possibility of structural features transverse to the main arc[3,11]. In view of this, we retain this direction and refer to it as the strike direction of a possible transverse geological structure in the southern part of the profile. Such transverse structure could be interpreted as an extension of the Aravalli trend into the Himalaya, i.e. THC[13]. Average geoelectric strike directions for major regions in the corridor are shown in Figure 3 by lines labelled a–f along with two boundaries shown by dotted lines – labelled g and h – indicating the extension of these features along the profile. This study suggests the following dimensionality and directionality features in the four lithotectonic regions in the GHC:

1. Southernmost region of the profile is represented by 1D structure in the period range 0.01–2 s. In this period range phase tensor ellipses have low ellipticity, approaching a circle and geoelectric strike is highly unstable. To relate this observed geoelectric dimensionality and strike direction to the geological features in depth, the period range is converted to an approximate depth using Niblett–Bostick method[29,30] and to an azimuthally invariant determinant impedance response. Accordingly, this region represents 1D sedimentary structure in the southern part of the profile and is extended to a depth of about 6 km. This depth range of the IGP sediments is consistent with the 2D geoelectrical model of the region[28].

2. Below the IGP sediments, the structure is represented by 2D with an average strike of N13°E at 15 sites in the period band of 13–1024 s. This period bandwidth decreases from 13–1024 s in the IGP to 256–1024 s in the northern end. Depth conversion indicates that the top of this transverse structure with a strike of N13°E is dipping at an angle of approximately is ~23° toward NNE. This feature appears at 15 sites in the MT data and thus is significant for the present dataset. This feature, nearly transverse to the main Himalaya arc, shows parallelism with the Aravalli trends. A similar feature was postulated by Valdiya[3] and Auden[4]. Subsequently, it was termed as Trans-Himalayan Conductor by Arora and Adam[13].

3. The other dominant geoelectric strike directions observed in the MT data corresponding to that of major thrusts (MFT, MBT and MCT) as shown in Figure 3, and labelled as b–d are N72°W ± 8°, N70°W ± 3°, and N71°W ± 6° respectively. It can be seen that uncertainty in the strike values is more in the southern- and northernmost regions for MFT and MCT. Higher uncertainty is due to the instability in the strike direction in the southern end (1D sedimentary structure in the IGP) and presence of multi-conductor with non-parallel strike in the MCT zone.

4. Besides the above features in the region, two features trending NNW direction are also observed in the SH and MCT zone and interpreted as localized fractures in the region. These features are labelled as 'a' and 'e' in Figure 3. The feature 'a' in the MCT zone with strike of N24°W ± 7° appears to be correlated with strike of focal plane of Uttarakashi earthquake of 19 October 1991 (ref. 31). Strong ground motion study[31] of Uttarkashi earthquake revealed that strike of the focal plane NP1 is N28°W, which closely matches with feature 'a' in Figure 3. Another similar feature identified by character 'e' has a strike of N10°W ± 5°. To further study transverse conducting feature in the GHC corridor, we discuss 3D modelling of tipper response in the following section.

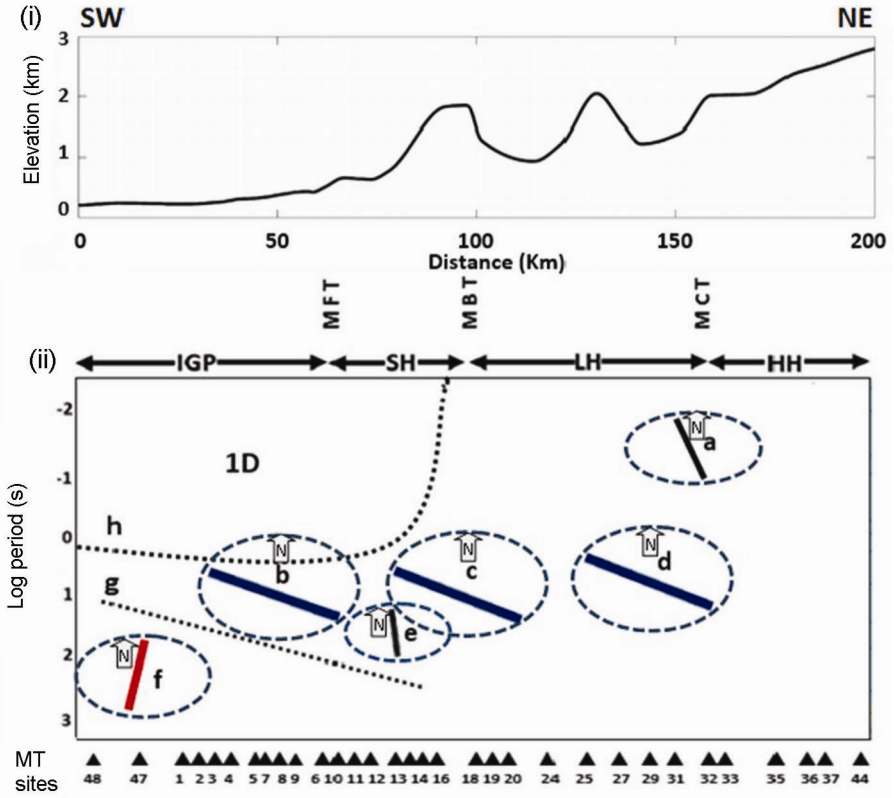

Figure 3. (i) Elevation plot along Roorkee–Gangotri profile. (ii) Geoelectric strike variation along the profile in four lithotectonic regions: the strike directions are shown by six different bars labelled 'a' to 'f' in ellipse insets. The orientation (with respect to north indicated in each inset) of these bars signifies the strike direction of the features in each region. For the features 'a'–'e' extension of the bars along the *x*-axis additionally illustrates the sites where these features are sensed. However, feature 'f', is sensed on sites lying within the horizontal range of the dotted line 'g', which also defines period sensitive to the top boundary surface of this transverse feature. The short-period region in the southwest (SW) of the profile, bounded by the dotted line 'h' represents 1D structure.

Three-dimensional modelling of tipper response

The tipper vector in magnetotellurics defines tipping of the horizontal components of magnetic field vectors and is also known as induction vector in the geomagnetic depth sounding literature[13]. It can be defined in a horizontal plane in terms of a linear relationship between horizontal (H_x, H_y) and vertical magnetic (H_z) field components as:

$$H_z = T_{zx}H_x + T_{zy}H_y, \quad (2)$$

where T_{zx} and T_{zy} are components of the tipper. In frequency domain these are complex quantities represented in terms of real and imaginary components. Amplitude and direction of the tipper vector can be defined as:

$$|\mathrm{Re}\ T| = \mathrm{sqrt}((\mathrm{Re}\ T_{zx})^2 + (\mathrm{Re}\ T_{zy})^2), \quad (3)$$

and

$$T\_\mathrm{anlge} = (180/\mathrm{pi}) * \mathrm{phase}(\mathrm{Re}\ T). \quad (4)$$

Tipper vector is sensitive to the lateral electrical inhomogeneities and it can be used to locate conductive structure in a region. Real tipper vectors in Parkinson[32] convention point towards the zone of high conductivity, whereas in Weise convention they point away from the zone of high conductivity. In the following we model tipper response recorded from the GHC.

Using the MT data recorded from the GHC, stable tipper responses have been estimated at 26 sites. Figure 1 shows location of these sites. Figure 4 *a* is a plot of the real tipper in the Weise convention at a representative period (1024 s). It is observed that tipper vector is consistently trending toward the northwest direction at greater than 100 s period. This behaviour is observed at 15 sites located in the IGP, SH and at a few sites in the LH. This behaviour of tipper suggests the existence of a conductive structure oriented in southeast direction and continuing nearly parallel to the profile in the IGP to LH regions. To further study the possible causes of tipper vector behaviour, 3D modelling was performed to fit the observed tipper amplitude and direction of tipper with those modelled by adjusting the parameters (depth, conductivity, thickness

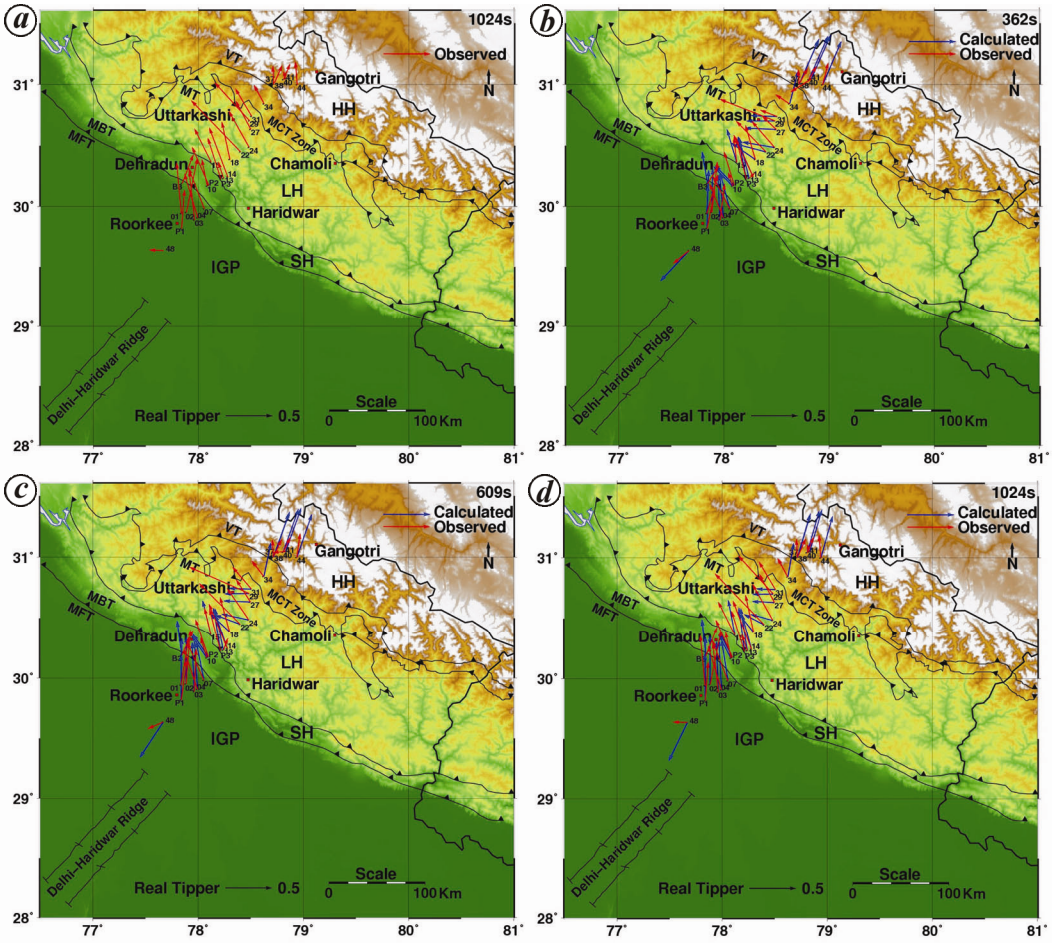

Figure 4. Observed and computed tipper response for selected period. ***a***, Observed tipper response at 1024 s period. ***b–d***, Comparison of observed and computed tipper at 362, 609 and 1024 s respectively.

and length) of the conductor by trial and error method. The directions of observed and computed tipper are also matched through the similarity index, C_n, defined as

$$C_n = \cos\theta = \frac{T_{\text{obs}} T_{\text{cal}}}{|T_{\text{obs}}||T_{\text{cal}}|}, \tag{5}$$

where T_{obs} and T_{cal} are observed and computed tipper respectively.

Initial 3D geoelectrical model has been constructed using simplified 2D block model obtained through 2D inversion of MT data[28] and by incorporating a conducting body to the southeast and parallel to the profile as indicated by tipper behaviour. Figure 5 *a* and *b* shows *XY* planes at surface (zero depth) and 20 km depth of 3D model respectively, obtained after fitting the tipper vector. Figure 4 *b–d* shows the corresponding observed and computed tipper at three representative periods. It may be mentioned here that 3D modelling is performed by incorporating the broad feature of the 2D model and transverse conducting feature. Parameters of the 3D model are adjusted manually to improve the fit between the observed and computed tipper responses. Fit between the observed and computed responses is generally improved with this experiment. However, the fitting is poor for sites located in the northern region. This may be due to ambiguous behaviour of the tipper in the presence of multiple conductors with non-parallel strikes[13]. Similarity index (Figure 6) is also poor at the site in the MCT zone. These observations suggest the existence of transverse conductor in the GHC along with other conducting features associated with the thrust zones along the main Himalayan arc. These two are nearly perpendicular in nature and hence explain transverse tectonics in the GHC.

Discussion and conclusion

Geoelectric structure dimensionality and directionality analysis indicates the existence of transverse and oblique features in addition to the main Himalayan arc in the GHC. Three such features, one transverse feature in the IGP and two oblique features in the SH and MCT zone, are delineated in the present analysis. The transverse feature in the IGP continues to the northeast (N13°E) in

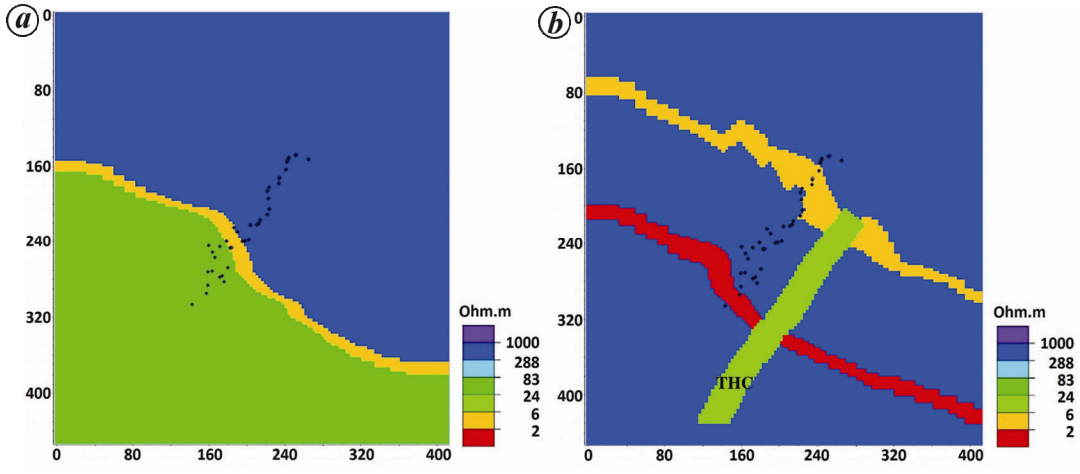

Figure 5. ***a***, Electrical structure of top surface layer (*xy*-plane) of simplified 3D model slice. ***b***, Electrical structure at 20 km depth (*xy*-plane) of simplified 3D model slice. Trans-Himalayan conductor fitted by tipper responses is indicated as THC.

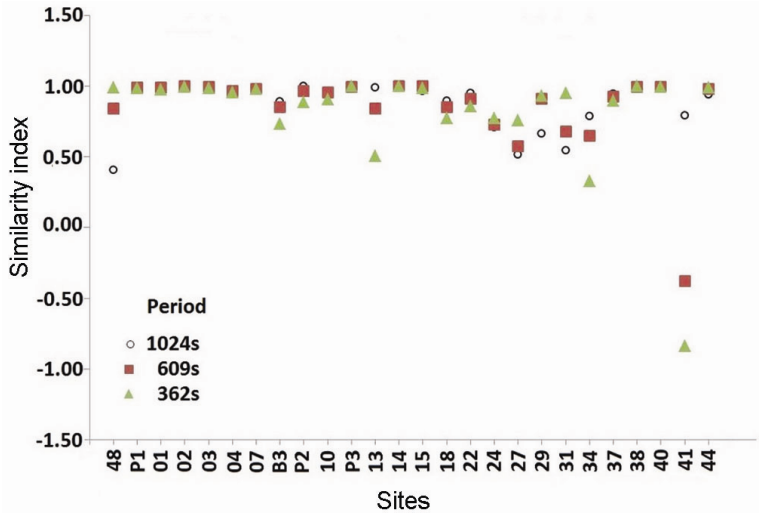

Figure 6. Similarity index computed between observed and fitted tipper responses at representative periods.

the SH and LH domain. Such a feature was earlier indicated in the literature and is related with the possible extension of the Aravalli[3]. Whereas two oblique features, aligned with a strike of N10°W in the SH and N24°W in the MCT zone, are local in nature. These appear to be associated with fault planes of possible past earthquakes in the region. The strike of the MCT zone feature is consistent with that of the fault plane of Uttarakashi earthquake of 19 October 1991 (ref. 31).

The tipper response also supports the existence of transverse conducting feature in the region. The 3D tipper modelling approach was used to present geoelectrical model of the region. Initial model for this study has been developed by transforming a 2D geoelectrical model into a simplified block model and by adding in it a 3D feature consistent with the tipper response and transverse strike in the IGP region. Parameters of the additional transverse conducting structure have been adjusted iteratively by fitting observed and computed tipper responses. Due to the presence of multi-conductors with non-parallel strike, good fitting could not be achieved at all sites. Following are the main features of the final 3D geoelectrical model obtained by this experiment.

The IGP sediments extend from the southernmost end of the model domain with 6 km thickness and resistivity of 30 Ohm-m. Further north of the IGP formation resistivity is 5 Ohm-m, representing the MBT. Ramp structure near the MCT in the depth range from 6 to 30 km is modelled in three steps. The MCT conductor with resistivity 4 Ohm-m has been added in the MCT zone. THC with a resistivity of 10 Ohm-m is extended from the southern end of the profile to the MCT zone in the north, parallel

and 50 km east of the existing MT profile. The thickness of the THC is 15 km which is adjusted in the depth range from 15 to 30 km to fit the computed tipper with that observed. The proposed 3D model of the study region is generated from a limited set of MT data, which needs to be further improved by adding more MT sites and by conducting full 3D inversion of the complete dataset.

1. Le Fort, P., Himalaya: the collided range. Present knowledge of the continental arc. *Am. J. Sci.*, 1975, **275**, 7–44.
2. Molnar, P., A review of the seismicity and the rate of active underthrusting and deformation at the Himalaya. *J. Himalayan Geol.*, 1990, **1**(2), 131–154.
3. Valdiya, K. S., Himalayan transverse faults and folds and their parallelism with subsurface structures of North Indian Plains. *Tectonophysics*, 1976, **32**, 353–386.
4. Auden, J. B., Transverses in the Himalaya. *Rec. Geol. Surv. India*, 1935, **69**, 123–167.
5. Larson, K. M., Burgmann, R., Bilham, R. and Freymueller, J., Kinematics of the India–Eurasia collision zone from GPS measurements. *J. Geophys. Res*., 1999, **104**, 1077–1093.
6. Banerjee, P., Bürgmann, R., Nagarajan, B. and Apel, E., Intraplate deformation of the Indian subcontinent. *Geophys. Res. Lett.*, 2008, **35**, L18301.
7. Duncan, C., Masket, J. and Fielding, E., How steep are the Himalaya? Characteristics and implications of along-strike topographic variations. *Geology*, 2003, **31**, 75–78.
8. Yin, A., Cenozoic tectonic evolution of the Himalayan orogen as constrained by along-strike variation of structural geometry, exhumation history, and foreland sedimentation. *Earth Sci. Rev.*, 2006, **76**, 1–131.
9. Burgess, W. P., Yin, A., Dubey, C. S., Shen, Z.-K. and Kelty, T. K., Holocene shortening across the Main Frontal Thrust zone in the eastern Himalaya. *Earth Planet. Sci. Lett.*, 2012, **357–358**, 152–167.
10. Mitra, S., Sribharath, M. K., Amit Padhi, R. S. S. and Bhattacharya, S. N., The Himalayan foreland basin crust and upper mantle. *Phys. Earth Planet. Inter.*, 2011, **184**, 34–40.
11. Khattri, K. N. and Tyagi, A. K., Seismicity pattern in the Himalayan plate boundary and identification of the areas of high seismic potential. *Tectonophysics*, 1983, **96**, 281–297.
12. Godin, L. and Harris, L. B., Tracking basement cross-strike discontinuities in the Indian crust beneath the Himalayan orogen using gravity data – relationship to upper crustal faults. *Geophys. J. Int.*, 2014, **198**, 198–215.
13. Arora, B. R. and Adam, A., Anomalous directional behaviour of induction arrows above elongated conductive structures and its possible causes. *Phys. Earth Planet. Inter.*, 1992, **74**, 183–190.
14. Manglik, A., Pavan Kumar, G. and Thiagrajan, S., Transverse tectonics in the Sikkim Himalaya: a magnetotelluric study. *Tectonophysics*, 2013, **589**, 142–150.
15. Valdiya, K. S., Reactivation of Himalayan Frontal Fault. *Curr. Sci*., 2003, **85**, 1031–1040.
16. Khattri, K. N., Local seismic investigations in the Garhwal–Kumaun Himalaya. *Mem. Geol. Soc. India*, 1992, **23**, 45–66.
17. Valdiya, K. S., *Geology of the Kumaon Lesser Himalaya*, Wadia Institute of Himalayan Geology, Dehra Dun, 1980, p. 291.
18. Gupta, S., Mahesh, P., Sivaram, K. and Rai, S. S., Active fault beneath the Tehri dam, Garhwal Himalaya – seismological evidence. *Curr. Sci.*, 2012, **103**(11), 1343–1347.
19. Mahesh, P., Rai, S. S., Sivaram, K., Paul, A., Sandeep Gupta, Sarma, R. and Gaur, V. K., One dimensional reference velocity model and precise locations of earthquake hypocenters in the Kumaon–Garhwal Himalaya. *Bull. Seismol. Soc. Am.*, 2013, **103**(1), 328–339.
20. Qureshy, M. N., Thickening of the basaltic layer as a possible cause for the uplift of the Himalayas – a suggestion based on gravity data. *Tectonophysics*, 1969, **7**, 137–157.
21. Weaver, J. T., Agarwal, A. K. and Lilley, F. E. M., Characterization of the magnetotelluric tensor in terms of its invariants. *Geophys. J. Int*., 2000, **141**, 321–336,
22. Caldwell, T. G., Bibby, H. M. and Brown, C., The magnetotelluric phase tensor. *Geophys. J. Int.*, 2004, **158**, 457–469.
23. Martí, A., Queralt, P. and Ledo, J., WALDIM: a code for the dimensionality analysis of magnetotelluric data using the rotational invariants of the magnetotelluric tensor. *Comput. Geosci.*, 2009, **35**, 2295–2303.
24. Groom, R. W. and Bailey, R. C., Decomposition of magnetotelluric impedance tensors in the presence of local three-dimensional galvanic distortion. *J. Geophys. Res.*, 1989, **94**, 1913–1925.
25. Bahr, K., Interpretation of the magnetotelluric impedance tensor: regional induction and local telluric distortion. *J. Geophys.*, 1988, **62**, 119–127.
26. Bahr, K., Geological noise in magnetotelluric data: a classification of distortion types. *Phys. Earth Planet. Inter.*, 1991, **66**, 24–38.
27. Khattri, K. N., Great earthquakes, seismicity gaps, and potential for earthquake disaster along the Himalaya plate boundary. *Tectonophysics*, 1987, **138**, 79–92.
28. Miglani, R., Shahrukh, M., Israil, M., Gupta, P. K. and Varshney, S. K., Geoelectric structure estimated from magnetotelluric data from the Uttarakhand Himalaya, India. *J. Earth Syst. Sci.*, 2014, **123**, 1907–1918.
29. Bostick, F. X., A simple almost exact method of MT analysis. Workshop on Electrical Methods in Geothermal Exploration. *U.S. Geol. Surv.*, 1977, Contract No. 14080001-8-359.
30. Jones, A. G., On the equivalence of the 'Bostick' and 'Niblett' transformations in the magnetotelluric method. *J. Geophys.*, 1983, **53**, 72–73.
31. Yu, G., Khattri, K. N., Anderson, J. G., Brune, J. N. and Zeng, Y., Strong ground motion from the Uttarkashi, Himalaya, India, earthquake: comparison of observation with the synthetic using the composite source model. *Bull. Seismol. Soc. Am.*, 1995, **85**, 31–50.
32. Parkinson, W. D., The influence of continents and oceans on geomagnetic variations. *Geophys. J. R. Astron. Soc.*, 1962, **6**, 441–449.

ACKNOWLEDGEMENTS. We thank the Ministry of Earth Sciences, Government of India for financial support to carry out this work. We also thank Mr Sudhanshu Tyagi and Mr Manoj Kumar for help in recalculation of geoelectrical strike used in this paper.

Received 16 September 2015; revised accepted 26 April 2016

doi: 10.18520/cs/v111/i5/868-875